



Solutions of the Einstein Equations for a Black Hole Surrounded by a Galactic Halo

R. A. Konoplya¹ and A. Zhidenko²

¹ Research Centre for Theoretical Physics and Astrophysics, Institute of Physics, Silesian University in Opava, Bezručovo náměstí 13, CZ-74601 Opava, Czech Republic; alexandr.zhidenko@ufabc.edu.br

² Centro de Matemática, Computação e Cognição (CMCC), Universidade Federal do ABC (UFABC), Rua Abolição, CEP: 09210-180, Santo André, SP, Brazil
Received 2022 March 1; revised 2022 June 4; accepted 2022 June 6; published 2022 July 12

Abstract

Various profiles of matter distribution in galactic halos (such as the Navarro–Frenk–White, Burkert, Hernquist, Moore, Taylor–Silk models, and others) are considered here as the source term for the Einstein equations. We solve these equations and find exact solutions that represent the metric of a central black hole immersed in a galactic halo. Even though in the general case the solution is numerical, very accurate general analytical metrics, which include all the particular models, are found in the astrophysically relevant regime, when the mass of the galaxy is much smaller than the characteristic scale in the halo.

Unified Astronomy Thesaurus concepts: [Astrophysical black holes \(98\)](#); [General relativity \(641\)](#); [Galaxy dark matter halos \(1880\)](#)

1. Introduction

Almost every large galaxy has a supermassive black hole in its center (Kormendy & Ho 2013). Galactic matter is usually modeled by an anisotropic fluid with some density distribution, which implies an almost spherical halo dominated by dark matter (Benson 2010). Depending on the size, mass, and form of a galaxy one or another distribution is preferable. The generic density distribution of a galactic halo has the following form (see, e.g., Taylor & Silk 2003):

$$\rho(r) = 2^{(\gamma-\alpha)/k} \rho_a (r/a)^{-\alpha} (1 + r^k/a^k)^{-(\gamma-\alpha)/k}, \quad (1)$$

which interpolates between the slope α near the galactic center and the slope γ at large distance $r \gg a$. Here a is the characteristic scale of the galactic halo. For a dwarf galaxy, composed of about a thousand up to several billion stars, the Burkert model ($\alpha = 1$, $\gamma = 3$, $k = 2$; Burkert 1995; Salucci & Burkert 2000) is suitable, while for galaxies with the largest content of dark matter, the Navarro–Frenk–White model ($\alpha = 1$, $\gamma = 3$, $k = 1$; Navarro et al. 1995, 1997) is mostly used. The Hernquist profile ($\alpha = 1$, $\gamma = 4$, $k = 1$; Hernquist 1990) is applied for modeling the Sérsic profiles observed in bulges and elliptical galaxies. When supposing the cold dark-matter halos that form within cosmological N -body simulations, the Moore model ($\alpha = 7/5$, $\gamma = 14/5$, $k = 7/5$; Moore et al. 1998) is considered. Within supersymmetric models the lightest neutralino is an excellent candidate to form the universe's cold dark matter, and they can be observed indirectly owing to annihilation in regions of high dark-matter density, such as the centers of galactic halos (Feng 2010). When studying signals from such annihilation events, the Taylor–Silk model ($\alpha = 3/2$, $\gamma = 3$, $k = 3/2$; Taylor & Silk 2003) is suggested. Dynamical constraints on such dark-matter models of galaxies were studied in Lacroix (2018), while the impact of relativistic corrections on the detectability of dark-matter spikes with

gravitational waves were considered in Speeney et al. (2022). A general relativistic description of a black hole surrounded by a central region of a galaxy was given in Sadeghian et al. (2013).

The natural question in this context is whether we can ascribe a general relativistic metric to such galactic distribution of matter that includes the spacetime of a central black hole. One way is to consider an isolated black hole spacetime that is matched to some distribution of matter via the mass function (Hou et al. 2018; Xu et al. 2018; Konoplya 2019; Jusufi et al. 2020; Liu et al. 2021; Zhang et al. 2021, 2022). In contrast to such a cut-and-paste approach, a straightforward solution has been recently suggested in Cardoso et al. (2021) where the problem of general relativistic description of a central black hole immersed in the (Hernquist distribution) galactic halo was considered self-consistently, i.e., via a solution of the corresponding Einstein equations with the energy-momentum tensor representing the galactic matter. Quasi-normal modes, scattering, and optical phenomena for this solution have been studied in Konoplya (2021) and Stuchlik & Vrba (2021), while an exact solution for a different equation of state of the galactic matter was proposed in Jusufi (2022) in a similar fashion.

In the present paper we propose a general approach of this kind and find exact solutions of the Einstein equations with the energy-momentum tensor corresponding to various distributions of the galactic medium. Even though the analytical solutions can be obtained only in particular cases, we show that a very good analytical approximation can be obtained in the general case by expanding the accurate solution in terms of the small parameter M/a , where M is the mass of a galaxy.

Thus, for a spherically symmetric line element,

$$ds^2 = -f(r)dt^2 + \frac{dr^2}{1 - 2m(r)/r} + r^2(d\theta^2 + \sin^2\theta d\varphi^2), \quad (2)$$

where $m(r) < r/2$ is the mass function and $f(r) > 0$ is the redshift function, we find an analytical approximate form of the metric. In particular, we will show that the approximate metric takes the following compact form for the Navarro–Frenk–



Original content from this work may be used under the terms of the [Creative Commons Attribution 4.0 licence](#). Any further distribution of this work must maintain attribution to the author(s) and the title of the work, journal citation and DOI.

White model (Navarro et al. 1995, 1997),

$$\begin{aligned} f(r) &= \left(1 - \frac{r_0}{r}\right) \left(1 - \eta \left(\frac{a}{r} \ln \frac{a}{r+a} + \mu\right)\right), \\ 1 - \frac{2m(r)}{r} &= \left(1 - \frac{r_0}{r}\right) \left(1 - \eta \frac{a}{r+a} - \eta \frac{a}{r} \ln \frac{a}{r+a}\right), \\ \mu &= \frac{a}{a+s}, \\ \eta &= \frac{2Ms(a+s)}{a(s-r_0)(s+(a+s)\ln(a/(a+s)))}, \end{aligned} \quad (3)$$

and for the Burkert model (Burkert 1995; Salucci & Burkert 2000),

$$\begin{aligned} f(r) &= \left(1 - \frac{r_0}{r}\right) \left(1 - \eta \left(\frac{a}{2r} \ln \frac{r^2+a^2}{a^2} + \mu - \arctan \frac{r}{a}\right)\right), \\ 1 - \frac{2m(r)}{r} &= \left(1 - \frac{r_0}{r}\right) \left(1 - \eta \frac{a}{2r} \ln \frac{r^2+a^2}{a^2}\right), \\ \mu &= \arctan \frac{s}{a}, \quad \eta = \frac{4Ms}{a(s-r_0)\ln(1+s^2/a^2)}. \end{aligned} \quad (4)$$

Here s is the radius of the galactic halo and r_0 is the radius of the event horizon.

While for the model of Taylor & Silk (2003) the approximate analytic expression has a rather cumbersome form, for a Taylor–Silk–like model ($\alpha = 3/2$, $\gamma = 3$, $k = 1$), which provides the same slopes for the density distribution in the central and far regions (though with a slightly different interpolation between them), the corresponding metric functions are

$$\begin{aligned} f(r) &= \left(1 - \frac{r_0}{r}\right) \left(1 - \eta \left(\frac{a}{r} \operatorname{arcsinh} \sqrt{\frac{r}{a}} + \mu - \sqrt{\frac{r+a}{r}}\right)\right), \\ 1 - \frac{2m(r)}{r} &= \left(1 - \frac{r_0}{r}\right) \left(1 - \eta \frac{a}{r} \operatorname{arcsinh} \sqrt{\frac{r}{a}} - \sqrt{\frac{r}{r+a}}\right), \\ \mu &= \sqrt{\frac{s}{a+s}}, \quad \eta = \frac{2Ms}{a(s-r_0)(\operatorname{arcsinh} \sqrt{s/a} - \mu)}. \end{aligned} \quad (5)$$

We will show that for the general case given by Equation (1), the analytic approximation can be found in the form of the hypergeometric function.

2. Black Hole Surrounded by the Galactic Halo

We assume that Equation (2) is the solution to the Einstein equations with the stress-energy tensor corresponding to the anisotropic matter with the density $\rho(r)$ and only the tangential pressure $P(r)$,

$$T_0^0 = -\rho(r), \quad T_2^2 = T_3^3 = P(r). \quad (6)$$

The Einstein equations imply

$$m'(r) = 4\pi r^2 \rho(r), \quad \frac{f'(r)}{f(r)} = \frac{2m(r)}{r^2 - 2rm(r)}, \quad (7)$$

and the tangential pressure has the form,

$$P(r) = \frac{r\rho(r)}{2} \frac{m(r)}{r^2 - 2rm(r)}. \quad (8)$$

Thus, once the density distribution is specified, all the functions can be determined by solving Equations (7) with the following conditions:

$$m(0) = 0, \quad f(\infty) = 1. \quad (9)$$

We will consider the density distribution (1), where the constant $\rho_a \equiv \rho(a)$ fixes the total mass of the galaxy

$$M = m(s) = 4\pi \int_0^s \rho(r) r^2 dr, \quad (10)$$

and s is the radius of the halo, such that $s > a \gg M$. We notice that for $\gamma > 3$ the galaxy size can be taken infinite, since, as $s \rightarrow \infty$, the improper integral (Equation (10)) converges. When s is finite, in order to have a finite total mass, we suppose that the space is empty outside the galactic halo, i.e., $\rho(r > s) = 0$.

When there is a black hole in the center of the galaxy, the density distribution is modified near the event horizon, located at $r_0 \ll M$, in such a way that the galactic distribution of matter is reproduced in the far zone. In the general case we consider

$$\rho(r) \rightarrow \tilde{\rho}(r) = b(r)\rho(r), \quad (11)$$

where the prefactor $b(r)$ approaches unity for $r \gg r_0$. For this purpose we can define the function $b(r)$ through the following expansion:

$$b(r) = 1 + C_1 \frac{r_0}{r} + C_2 \frac{r_0^2}{r^2} + C_3 \frac{r_0^3}{r^3} + \dots \quad (12)$$

In particular, the choice

$$b(r) = (1 - r_0/r)^{n+1} \quad (13)$$

sets to zero the density and its first n derivatives at the event horizon. By solving Equations (7) with the following conditions (see Equation (9)),

$$m(r_0) = r_0/2, \quad f(\infty) = 1, \quad (14)$$

we obtain numerically the accurate metric functions describing the galactic halo with the central black hole of radius r_0 . For the Hernquist-type density distribution ($\alpha = 1$, $\gamma = 4$, $k = 1$) and $n = 0$ in Equation (13), the resulting metric has been obtained in an analytic form in Cardoso et al. (2021).

In order to simplify analysis in the general case, we introduce the new functions, $A(z)$ and $B(z)$, which are finite at the horizon,

$$\begin{aligned} f(r) &= \left(1 - \frac{r_0}{r}\right) A\left(\frac{r}{a}\right), \\ 1 - \frac{2m(r)}{r} &= \left(1 - \frac{r_0}{r}\right) B\left(\frac{r}{a}\right). \end{aligned} \quad (15)$$

The functions $A(z)$ and $B(z)$ are dimensionless and must depend on the following small dimensionless parameters: $\frac{M}{a}$, $\frac{r_0}{a}$ and $\frac{s}{a}$. For our purposes, we can safely ignore the dependence on the two latter parameters, since the black hole size is negligible

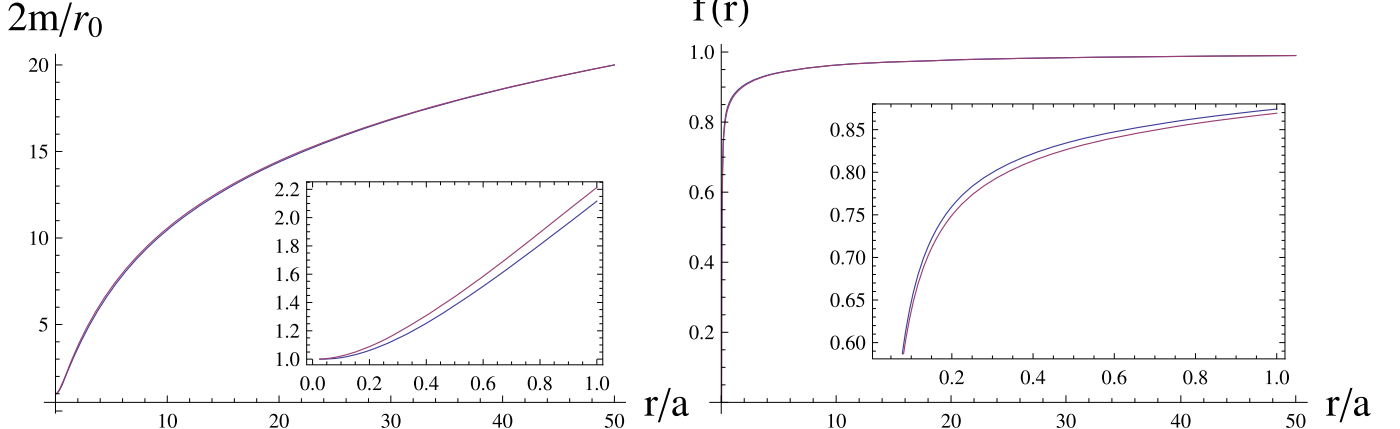


Figure 1. Comparison of the numerical solution of Equation (7) (blue) and the analytic expression, Equation (15) (red), for $a = 4M_t = 40r_0$, $s = 50a$ ($\alpha = 1$, $\gamma = 3$, $k = 1$).

comparing to the size of the galaxy. Therefore, we have

$$\begin{aligned} A(z) &= 1 - \frac{2M}{a}\tilde{A}(z) + \mathcal{O}\left(\frac{M}{a}\right)^2, \\ B(z) &= 1 - \frac{2M}{a}\tilde{B}(z) + \mathcal{O}\left(\frac{M}{a}\right)^2. \end{aligned} \quad (16)$$

We notice that in the region near the black hole, i.e., for $r \simeq r_0 \ll a$, the redshift function gains the factor

$$A\left(\frac{r}{a}\right) \approx A(0) = 1 - \frac{2M}{a}\tilde{A}(0), \quad (17)$$

which corresponds to the dominant redshift correction to the frequencies due to the galactic halo. Further, we shall calculate the value of $\tilde{A}(0)$ explicitly, and also note that $\tilde{B}(0) = 0$.

By solving Equations (7), taking the dominant order in $1/a$ and neglecting the terms of order r_0/a , we find that $\tilde{B}(z)$ does not depend on the particular choice of the prefactor $b(r)$ in Equation (11):

$$\begin{aligned} M\tilde{B}(z) &= \frac{4\pi\rho_a a^3}{3-\alpha} 2^{(\gamma-\alpha)/k} \\ &\times {}_2F_1\left(\frac{3-\alpha}{k}, \frac{\gamma-\alpha}{k}, \frac{3-\alpha}{k} + 1; -z^k\right) z^{2-\alpha}, \end{aligned} \quad (18)$$

where

$${}_2F_1(a, b, c; x) \equiv \sum_n \frac{\Gamma(a+n)\Gamma(b+n)\Gamma(c)}{\Gamma(a)\Gamma(b)\Gamma(c+n)} \cdot \frac{x^n}{n!}$$

is the hypergeometric function. Substituting Equation (15) into (7) and neglecting the black hole size as compared to the galactic scales, we obtain

$$A'(z) = A(z)(B^{-1}(z) - 1)/z, \quad (19)$$

which, after substitution of Equation (16), leads in the dominant order to the following relation:

$$\tilde{A}'(z) = -\tilde{B}(z)/z. \quad (20)$$

Using Equation (18) in (20) one can find explicitly $A(z)$ in terms of the generalized hypergeometric functions,

$$\begin{aligned} M\tilde{A}(z) &= \mu - \frac{4\pi\rho_a a^3}{3-\alpha} 2^{(\gamma-\alpha)/k} \\ &\times {}_2F_1\left(\frac{3-\alpha}{k}, \frac{\gamma-\alpha}{k}, \frac{3-\alpha}{k} + 1; -z^k\right) z^{1-\alpha} dz. \end{aligned} \quad (21)$$

The constant of integration μ is fixed in order to match the Schwarzschild geometry for $r > s$,

$$g_{tt} = -g_{rr}^{-1} = -1 + 2M_t/r, \quad r > s, \quad (22)$$

where $M_t = M + r_0/2$ is the total asymptotic mass. Thus, the values of ρ_a and μ are determined in terms of the asymptotic mass M_t and the cutoff parameter s by matching the Schwarzschild metric Equation (22) at $r = s$:

$$\tilde{A}\left(\frac{s}{a}\right) = \frac{a}{2M} \left(1 - \frac{s-2M_t}{s-r_0}\right) \approx \frac{a}{s}, \quad (23)$$

$$\tilde{B}\left(\frac{s}{a}\right) = \frac{a}{2M} \left(1 - \frac{s-2M_t}{s-r_0}\right) \approx \frac{a}{s}. \quad (24)$$

Even for quite large values of M/a the resulting analytic expressions approximate very well the accurate metric functions, which can be found only numerically (see Figure 1). For the particular cases of the Navarro–Frenk–White, Burkert, and Taylor–Silk–like models, the above hypergeometric functions take a relatively simple form leading to Equations (3)–(5) for the metric functions. The analytic approximation for the metric functions is available in the Wolfram Mathematica® ancillary file.³

We would like to note that within our approach the cutoff occurs not in an arbitrary place, but at the radius of the galactic halo. Outside this radius the (conditionally) empty space is described by the Schwarzschild metric produced by the total mass of the halo. Therefore, the results depend on the cutoff parameter exactly in the same way, as they depend on the size of the galaxy. If we fix the total mass and change the size of the galaxy (and consequently the value of s), we change the density of the halo, and the observables are changed correspondingly.

³ The ancillary file is available from <https://arxiv.org/src/2202.02205/anc>.

3. Circular Photon Orbit and ISCO

The shadow radius R_{sh} depends only on the redshift function $f(r)$, corresponding to the minimum

$$R_{sh} = \min_{r>r_0} \frac{r}{\sqrt{f(r)}} = \frac{r_{ph}}{\sqrt{f(r_{ph})}}, \quad (25)$$

where r_{ph} is the radius of the circular photon orbit. Substituting Equation (15) into (25) we find that

$$r_{ph}/r_0 = 3/2 + \mathcal{O}(r_0/a), \quad (26)$$

where we neglect the radius of the black hole as compared to the characteristic scale of the galaxy a . Therefore, we obtain the following expression for the shadow radius:

$$\begin{aligned} R_{sh} &= \frac{3r_0}{2\sqrt{f(3r_0/2)}} + \mathcal{O}\left(\frac{r_0}{a}\right) \\ &= \frac{3\sqrt{3}r_0}{2} \left(1 + \frac{M}{a}\tilde{A}(0) + \mathcal{O}\left(\frac{r_0}{a}\right) + \mathcal{O}\left(\frac{M}{a}\right)^2\right). \end{aligned} \quad (27)$$

Taking into account that Equation (18) implies $\tilde{B}(0) = 0$ ($\alpha < 2$), we obtain the Lyapunov exponent

$$\begin{aligned} \lambda &= \sqrt{\left(1 - \frac{2m(r_{ph})}{r_{ph}}\right) \frac{2f(r_{ph}) - f''(r_{ph})}{2r_{ph}^2}} \\ &= \frac{2}{3\sqrt{3}r_0} \left(1 - \frac{M}{a}\tilde{A}(0) + \mathcal{O}\left(\frac{r_0}{a}\right) + \mathcal{O}\left(\frac{M}{a}\right)^2\right). \end{aligned} \quad (28)$$

The radius of the innermost stable circular orbit r_{ISCO} satisfies the relation

$$\frac{3f'(r_{ISCO})}{r_{ISCO}} - \frac{2f'(r_{ISCO})^2}{f(r_{ISCO})} + f''(r_{ISCO}) = 0. \quad (29)$$

Substituting Equation (15) into (29) we obtain

$$r_{ISCO}/r_0 = 3 + \mathcal{O}(r_0/a)^{2-\alpha}. \quad (30)$$

Neglecting the black hole size as compared to the characteristic scale of the galaxy we find the corresponding frequency at ISCO,

$$\begin{aligned} \Omega_{ISCO} &= \sqrt{\frac{f'(r_{ISCO})}{2r_{ISCO}}} \\ &= \frac{1}{3\sqrt{6}r_0} \left(1 - \frac{M}{a}\tilde{A}(0) + \mathcal{O}\left(\frac{r_0}{a}\right) + \mathcal{O}\left(\frac{M}{a}\right)^2\right). \end{aligned} \quad (31)$$

It is well known that the high-frequency (eikonal) quasi-normal modes of test fields and, at least in a great number of cases, of gravitational perturbations are fully determined by the circular frequency and Lyapunov exponent of a null ray orbiting around the black hole (Cardoso et al. 2009; Konoplya & Stuchlik 2017). Thus, the quasi-normal frequencies in the eikonal regime ($\ell \rightarrow \infty$) and the ISCO frequency gain the same redshift due to the galactic halo with the factor $\tilde{A}(0)$, which

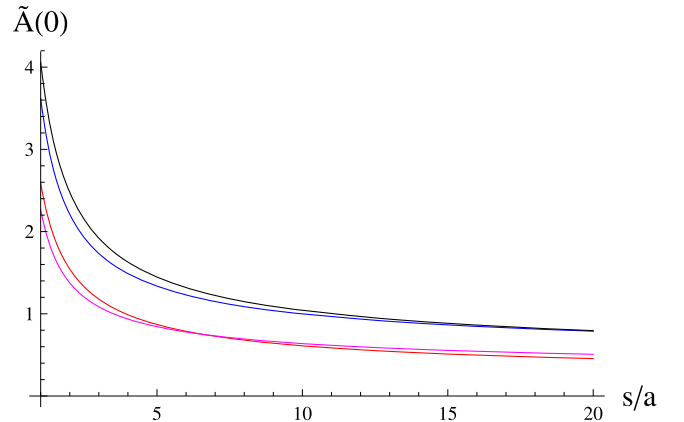


Figure 2. The redshift factor $\tilde{A}(0)$ as a function of the galactic size s for $\gamma = 3$: $\alpha = 1$, $k = 1$ (red) and $k = 2$ (magenta), $\alpha = 3/2$, $k = 1$ (black) and $k = 3/2$ (blue).

depends on s :

$$\tilde{A}(0) \approx \frac{(3-\alpha)a}{(2-\alpha)s} \frac{{}_2F_1\left(\frac{2-\alpha}{k}, \frac{\gamma-\alpha}{k}, \frac{2-\alpha}{k} + 1; -\left(\frac{s}{a}\right)^k\right)}{{}_2F_1\left(\frac{3-\alpha}{k}, \frac{\gamma-\alpha}{k}, \frac{3-\alpha}{k} + 1; -\left(\frac{s}{a}\right)^k\right)}. \quad (32)$$

For $\gamma = 3$, $\tilde{A}(0)$ goes to zero as s grows (see Figure 2), because the constant halo mass leads to the vanishing density in this limit. For $\gamma = 4$ in the limit $s \rightarrow \infty$ Equation (32) reads

$$s \lim_{s \rightarrow \infty} \tilde{A}(0) = \frac{(3-\alpha)\Gamma\left(\frac{2}{k}\right)\Gamma\left(\frac{2-\alpha}{k} + 1\right)}{(2-\alpha)\Gamma\left(\frac{1}{k}\right)\Gamma\left(\frac{3-\alpha}{k} + 1\right)}. \quad (33)$$

4. Accuracy of the Approximation

First of all, we will compare the analytic solution for the particular case of $\alpha = 1$, $\gamma = 4$, $k = 1$ (see Equation (6) of Cardoso et al. 2021) and our approximation, Equation (16), yielding

$$m(r) = \frac{r_0}{2} + \frac{Mr^2}{(r+a)^2} \left(1 - \frac{r_0}{r}\right), \quad (34)$$

which corresponds to the following density distribution (see Equation (10) of Cardoso et al. 2021)

$$4\pi\rho(r) = \frac{m'(r)}{r^2} = \frac{M}{r(r+a)^3} \left(2a + r_0 - \frac{ar_0}{r}\right). \quad (35)$$

Notice that $\rho(r_0) \neq 0$, because we have neglected some terms proportional to the black hole radius. The corresponding approximation for the redshift function takes the simple form

$$f(r) = \left(1 - \frac{r_0}{r}\right) \left(1 - \frac{2M}{r+a}\right), \quad (36)$$

which coincides with Equation (7) of Cardoso et al. (2021) within the considered approximation. The redshift factor (Equation (33)) for $\alpha = 1$, $\gamma = 4$, $k = 1$ is unity, so that for the eikonal quasi-normal modes and the ISCO frequency we

Table 1
Fundamental ($n = 0, \ell = 1$) Quasi-normal Mode of the Electromagnetic Field (in Units of r_0) Calculated for the Accurate Metric in Konoplya (2021) Compared to Time-domain Profile Values Found Using the Analytic Approximation for the Hernquist Model ($\alpha = 1, \gamma = 4, k = 1$)

a/r_0	$M = 5r_0$		$M = 10r_0$		$M = 50r_0$	
	Accurate	Approximation	Accurate	Approximation	Accurate	Approximation
1000	0.4940 – 0.1840 <i>i</i>	0.4940 – 0.1840 <i>i</i>	0.4916 – 0.1831 <i>i</i>	0.4916 – 0.1831 <i>i</i>	0.4719 – 0.1758 <i>i</i>	0.4711 – 0.1755 <i>i</i>
500	0.4916 – 0.1831 <i>i</i>	0.4916 – 0.1831 <i>i</i>	0.4866 – 0.1813 <i>i</i>	0.4865 – 0.1812 <i>i</i>	0.4479 – 0.1668 <i>i</i>	0.4443 – 0.1654 <i>i</i>
100	0.4723 – 0.1758 <i>i</i>	0.4715 – 0.1754 <i>i</i>	0.4485 – 0.1668 <i>i</i>	0.4451 – 0.1653 <i>i</i>	0.2741 – 0.1013 <i>i</i>	0.0657 – 0.0164 <i>i</i>

Note. The QNMs are computed via the WKB method (Schutz & Will 1985; Iyer & Will 1987; Konoplya 2003; Matyjasek & Opala 2017; Konoplya et al. 2019).

Table 2
Fundamental ($n = 0, \ell = 1$) Quasi-normal Mode of the Electromagnetic Field (in Units of r_0) Calculated via the WKB Approach for the Accurate Metric Numeric Metric ($b(r) = 1 - r_0/r$) Compared to the Values Found Using the Analytic Approximation ($\alpha = 1, \gamma = 3, s = 10a$) for the Navarro–Frenk–White ($k = 1$) and Burkert ($k = 2$) Models

$k = 1$	$M = 5r_0$		$M = 10r_0$		$M = 50r_0$	
	a/r_0	Accurate	Approximation	Accurate	Approximation	Accurate
1000	0.4940 – 0.1840 <i>i</i>	0.4940 – 0.1840 <i>i</i>	0.4935 – 0.1838 <i>i</i>	0.4935 – 0.1838 <i>i</i>	0.4815 – 0.1793 <i>i</i>	0.4812 – 0.1792 <i>i</i>
500	0.4935 – 0.1838 <i>i</i>	0.4935 – 0.1838 <i>i</i>	0.4905 – 0.1827 <i>i</i>	0.4905 – 0.1827 <i>i</i>	0.4666 – 0.1738 <i>i</i>	0.4653 – 0.1733 <i>i</i>
100	0.4816 – 0.1793 <i>i</i>	0.4813 – 0.1792 <i>i</i>	0.4668 – 0.1738 <i>i</i>	0.4655 – 0.1732 <i>i</i>	0.3543 – 0.1316 <i>i</i>	0.3118 – 0.1152 <i>i</i>

$k = 2$	$M = 5r_0$		$M = 10r_0$		$M = 50r_0$	
	a/r_0	Accurate	Approximation	Accurate	Approximation	Accurate
1000	0.4950 – 0.1844 <i>i</i>	0.4950 – 0.1844 <i>i</i>	0.4934 – 0.1838 <i>i</i>	0.4934 – 0.1838 <i>i</i>	0.4808 – 0.1791 <i>i</i>	0.4805 – 0.1790 <i>i</i>
500	0.4934 – 0.1838 <i>i</i>	0.4934 – 0.1838 <i>i</i>	0.4902 – 0.1826 <i>i</i>	0.4902 – 0.1826 <i>i</i>	0.4652 – 0.1733 <i>i</i>	0.4638 – 0.1728 <i>i</i>
100	0.4808 – 0.1791 <i>i</i>	0.4805 – 0.1789 <i>i</i>	0.4652 – 0.1732 <i>i</i>	0.4640 – 0.1727 <i>i</i>	0.3460 – 0.1286 <i>i</i>	0.3001 – 0.1111 <i>i</i>

have (see Equations (12) and (16) of Cardoso et al. 2021)

$$\Omega = \Omega_0(1 - M/a + \mathcal{O}(r_0/a) + \mathcal{O}(M/a)^2).$$

Comparison of the metric coefficients of the accurate numerical or analytical solution and the approximate one is not meaningful, because the metric coefficients are not observable gauge invariant characteristics. Instead we will compare the dominant proper oscillation frequencies, called *quasi-normal modes* (QNMs; Konoplya & Zhidenko 2011; Kokkotas & Schmidt 1999), which are sensitive to the near-horizon behavior. From the Table 1 we see that the approximation provides good estimations for the QNMs for the electromagnetic perturbations, even for large black holes ($M = 5r_0$) as long as M/a is small. We observe a similar behavior for the other models, examples of which are shown on Tables 2 for the Navarro–Frenk–White and Burkert profiles.

5. Conclusions

When constructing the metric of a supermassive black hole immersed in the galactic halo, a cut-and-paste approach is usually used, which simply matches the Schwarzschild solution with the weak field regime matter distribution via the mass function. On the contrary to this approach, here we developed the fully general relativistic approach and found self-consistent solutions to the Einstein equations describing a black hole immersed in some general distribution of matter (Equation (1)), which includes various profiles used for modeling the galactic halo. In the astrophysically motivated range of parameters the general analytical expression for the metric functions has been obtained in the form of the hypergeometric functions and the excellent accuracy of this expression is confirmed via analysis of

electromagnetic QNMs, frequencies at ISCO, and the radius of the black hole shadow. Even though the influence of the galactic environment is relatively small for the radiation processes around central black holes, they might be potentially observable in future, for example, when detecting QNMs, due to many cycles of rotation of a binary system before the merger in the galactic medium (Cardoso et al. 2021) or in optical phenomena owing to the dark-matter spikes in the central region (Nampalliwar et al. 2021). The current and expected-in-the-near-future sensitivity of the gravitational wave detectors is certainly not sufficient to detect the influence of the galactic environment.

A.Z. was supported by Conselho Nacional de Desenvolvimento Científico e Tecnológico (CNPq). R.K. would like to acknowledge support of the grant 19-03950S of Czech Science Foundation (GAČR).

ORCID iDs

R. A. Konoplya  <https://orcid.org/0000-0003-1343-9584>
A. Zhidenko  <https://orcid.org/0000-0001-6838-3309>

References

Benson, A. J. 2010, *PhR*, **495**, 33
 Burkert, A. 1995, *ApJL*, **447**, L25
 Cardoso, V., Destounis, K., Duque, F., Macedo, R. P., & Maselli, A. 2021, arXiv:2109.00005
 Cardoso, V., Miranda, A. S., Berti, E., Witek, H., & Zanchin, V. T. 2009, *PhRvD*, **79**, 064016
 Feng, J. L. 2010, *ARA&A*, **48**, 495
 Hernquist, L. 1990, *ApJL*, **356**, 359
 Hou, X., Xu, Z., Zhou, M., & Wang, J. 2018, *JCAP*, **07**, 015
 Iyer, S., & Will, C. M. 1987, *PhRvD*, **35**, 3621

Jusufi, K. 2022, arXiv:[2202.00010](#)

Jusufi, K., Jamil, M., & Zhu, T. 2020, *EPJC*, **80**, 354

Kokkotas, K. D., & Schmidt, B. G. 1999, *LRR*, **2**, 2

Konoplya, R. A. 2003, *PhRvD*, **68**, 024018

Konoplya, R. A. 2019, *PhLB*, **795**, 1

Konoplya, R. A. 2021, *PhLB*, **823**, 136734

Konoplya, R. A., & Stuchlik, Z. 2017, *PhLB*, **771**, 597

Konoplya, R. A., & Zhidenko, A. 2011, *RvMP*, **83**, 793

Konoplya, R. A., Zhidenko, A., & Zinhailo, A. F. 2019, *CQGra*, **36**, 155002

Kormendy, J., & Ho, L. C. 2013, *ARA&A*, **51**, 511

Lacroix, T. 2018, *A&A*, **619**, A46

Liu, D., Yang, Y., Wu, S., et al. 2021, *PhRvD*, **104**, 104042

Matyjasek, J., & Opala, M. 2017, *PhRvD*, **96**, 024011

Moore, B., Governato, F., Quinn, T. R., Stadel, J., & Lake, G. 1998, *ApJL*, **499**, L5

Nampalliwar, S., Kumar, S., Jusufi, K., et al. 2021, *ApJ*, **916**, 116

Navarro, J. F., Frenk, C. S., & White, S. D. M. 1995, *MNRAS*, **275**, 720

Navarro, J. F., Frenk, C. S., & White, S. D. M. 1997, *ApJ*, **490**, 493

Sadeghian, L., Ferrer, F., & Will, C. M. 2013, *PhRvD*, **88**, 063522

Salucci, P., & Burkert, A. 2000, *ApJL*, **537**, L9

Schutz, B. F., & Will, C. M. 1985, *ApJL*, **291**, L33

Speeney, N., Antonelli, A., Baibhav, V., & Berti, E. 2022, arXiv:[2204.12508](#)

Stuchlik, Z., & Vrba, J. 2021, *JCAP*, **11**, 059

Taylor, J. E., & Silk, J. 2003, *MNRAS*, **339**, 505

Xu, Z., Hou, X., Gong, X., & Wang, J. 2018, *JCAP*, **09**, 038

Zhang, C., Zhu, T., Fang, X., & Wang, A. 2022, arXiv:[2201.11352](#)

Zhang, C., Zhu, T., & Wang, A. 2021, *PhRvD*, **104**, 124082